LUND UNIVERSITY

Dynamic multi-link indoor MIMO measurements at 5.3 GHz.

Koivunen, Jukka; Almers, Peter; Kolmonen, Veli-Matti; Salmi, Jussi; Richter, Andreas; Tufvesson, Fredrik; Suvikunnas, Passi; Molisch, Andreas; Vainikainen, Pertti

DYNAMIC MULTI-LINK INDOOR MIMO MEASUREMENTS AT 5.3 GHz

J. Koivunen*, **P. Almers**[†], **V.-M. Kolmonen***, **J. Salmi**[‡], **A. Richter**[‡],
F. Tufvesson[†], **P. Suvikunnas***, **A. F. Molisch**[†§] **and P. Vainikainen***

*TKK Helsinki University of Technology, SMARAD Radio Laboratory, Finland
[†]Lund University, Dept. of Electrical and Information Technology, Sweden
[‡]TKK Helsinki University of Technology, SMARAD Signal Processing Laboratory, Finland
[§]Mitsubishi Electric Research Laboratories (MERL), Cambridge, MA, USA

Email: jukka.koivunen@tkk.fi
Fax:+358-9-4512152

Keywords: MIMO, multi-link, measurements, interference, capacity

Abstract

A dynamic multi-link MIMO channel indoor measurement campaign at 5.3 GHz is presented in this paper. The system setup is described and capacity with interference (with and without power control) results based on the dynamic multi-link MIMO measurements are shown, and we experience a strong correlation between the relative capacity and SIR. Furthermore, an interference suppression metric is introduced and pathloss exponents and delay spreads are also presented, when moving from a typical office corridor to a large entrance hall at the premises of Lund University, Sweden.

1 Introduction

With the constantly growing need for higher data rates, the shown potential of single link multiple-input multiple-output (MIMO) technology has drawn huge attention from the wireless community during the last ten years [13, 9, 5]. Already today some WLAN products (e.g., Draft 802.11n) utilizing the MIMO technology are available. The density of different wireless networks such as WLAN and WiMAX is increasing, and with the increased number of MIMO products the need to understand the effects of multi-user interference in multi-link MIMO scenarios is growing.

The capacity regions of multi-link MIMO have been extensively studied theoretically for both the downlink [4, 14, 12] and uplink [11, 9, 15]. In [3] the optimum signaling in terms of system capacity is derived. In addition to the theoretical work of multi-link MIMO channels, channel measurements are needed to extend the understanding of those channels.

Today, there exists some *static* multi-link MIMO measurements, where several single-link MIMO measurements have been taken and used to form a static multi-link scenario [6]. In this paper we describe a measurement setup capable of measuring the *dynamic* multi-link MIMO channel. To the best of our knowledge, this is the first dynamic multi-link MIMO measurement campaign published. We also present capacity with interference result, based on the dynamic multi-link measurements, as well as path-loss and delay spreads for the measured scenarios. Finally, we give a simple interference suppression metric.

The paper is structured as follows. In Section 2 the measurement setup is described, and in Section 3 the measurement scenarios are briefly presented. Results based on the measurement are presented in Section 4, and, finally, section 5 concludes the paper.

2 Measurement Setup

2.1 The LU and TKK Sounders

The receiver of the TKK sounder [7] is basically a down converter and sampling unit and all the signal processing, including the correlation of the received signal with the transmission signal, is done in a post processing process. Hence, the post-processing can be easily adjusted for other types of sounding signals.

The Lund University (LU) sounder is a commercial RUSK [10, 1] channel sounder produced by MEDAV GmbH. It uses fast RF switching and periodic multi-frequency signals. The transmitter of the LU sounder has an arbitrary waveform generator unit for generating periodic multi-frequency signals.

In Table 2.1 some specifications of the sounders are presented.

Using the waveform generator the bandwidth of the signal and its frequency response can be adjusted, and the center frequency and bandwidth of the LU sounder can be tuned to match those of the TKK sounder. Also the bandwidth of the transmission signal can be adjusted so that it can be measured with the sampling rate of the TKK receiver without aliasing.

Parameter	LU-sounder	TKK-sounder
f_c	5150 - 5750 MHz	5300 MHz
BW	10 - 240 MHz	120 MHz
TX-code length	1.6 μs	N/A
Sampling rate at TX	320 MHz	N/A
Sampling rate at RX	640 MHz	120 MHz
RX-element switching interval	3.2 μs	3.2 μs
Time between MIMO snapshots	39.3216 ms	39.3216 ms

TABLE I.   Sounder specifications

2.2 Synchronization

There are different levels of synchronization. In this setup the local oscillators are synchronized by using a common 10 MHz reference signal or synchronized Rubidium clocks making the impulse responses not to slide [2]. However, synchronization of the transmit signals, synchronization of antenna switching and synchronization of MIMO snapshots is not possible between the sounders which introduces a couple of issues that had to be solved.

1) since the transmit signals of the two transmitters can not be synchronized, orthogonality between TX signals (e.g., TDD) is not possible for a fast system. The measurement configuration is then limited to one TX and two RXs, as shown in Fig. 1, which is capable of measuring the dynamic *point-to-multi-point* and also *multi-point-to-point* MIMO channels (assuming channel reciprocity).
2) the transmit signals are not synchronized to the TKK RX, and therefore there exists a time difference between the LU and TKK channels (T_{SL} in Fig. 2). This time difference is not known, but will stay constant during a measurement and also between the measurements (unless the sounders are shut down) and is adjusted in the post-processing.
3) the LU TX switch and the TKK RX switch are not synchronized, resulting in that the channels are mixed up. This was solved by using a matched load at one of the TX channels and at one of the TKK RX channels, which makes it possible to synchronize the switching patterns in the post-processing using these dummy channels.
4) the start of a measurement is not synchronized between the LU TX and the TKK RX, hence the mapping of the MIMO snapshots of the LU TX with the MIMO snapshots of the TKK RX was solved by using a switch in the LU TX. Hence, in all of the measurements the transmitter power was switched on shortly after the sampling was started at both receivers. Using the snapshots where the power is switched on as a reference, the MIMO snapshots of the TKK and LU sounders can be synchronized in the post-processing.

2.3 Antennas

The antenna structures used in the measurement system are shown in Fig. 3.
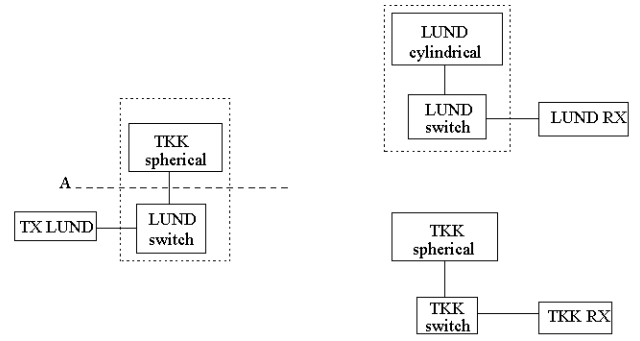

Fig. 1.   Block diagram of the dual-sounder measurements setup.
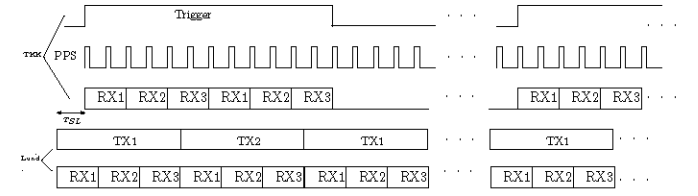

Fig. 2.   Synchronization between LU and TKK sounders shown for a 2 TX and 3 RX channel scenario.

The cylindrical antenna structure used at the LU RX consists of 4 rings of 8 dual polarized antenna elements, and so the antenna has 64 dual polarized (horizontal and vertical) antenna elements in total. From these, 16 dual polarized elements were used; 8 elements from each of the two middle rows was selected in an alternating fashion.

The semi-spherical antenna structure at the TKK RX has 21 dual polarized (horizontal and vertical) elements, of which 15 dual polarized elements are connected to the switch. In addition to these 30 channels a discone antenna (connected to the AGC controller of the TKK RX) and a dummy channel (for synchronization discussed previously) were used both at the LU TX and at the TKK RX.

The semi-spherical antenna structure used at the LU TX is almost identical to the one used in the TKK RX, except the polarization of the dual polarized elements is different (45° slanted). Here, 7 dual polarized elements of the TX antenna group were used together with a discone antenna and a dummy channel.

All unused antenna elements were terminated using matched loads.

3 Measurement Scenarios

An indoor measurement campaign was carried out in the E-building of Lund University during May 2007. In this paper we focus on the entrance hall – corridor scenario shown in Fig. 4 and Fig. 5. The long entrance hall is surrounded by corridors and lecture halls built by brick walls, which is also

Fig. 3. Picture of the antenna structures and switches. (left) LU TX switch together and TKK semi-spherical antenna structure, (middle) TKK RX switch and TKK semi-spherical antenna structure and (right) the LU RX switch and LU cylindrical antenna structure.
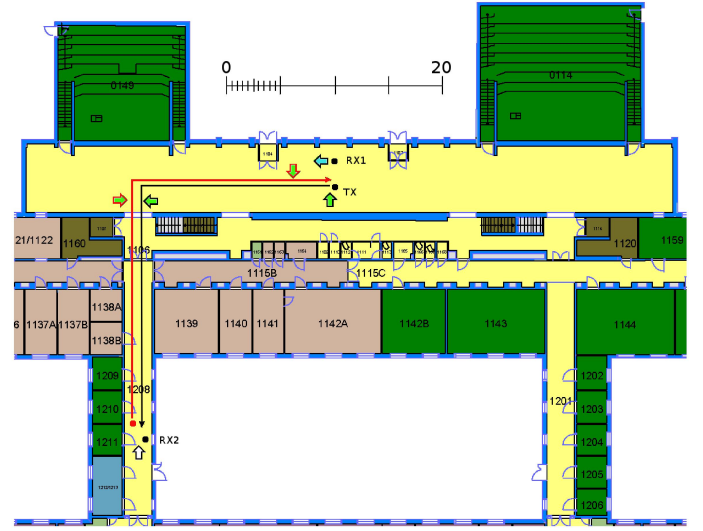
similar to e.g., an airport terminal, or a part of a shopping mall. In the measurement, the RX1 (LU RX) was located in the middle of the entrance hall and the RX2 (TKK RX) was located in a nearby corridor (see Fig. 5). This type of measurement scenario represents a real life application with two WLAN base stations, one in the entrance hall and one in the neigbouring corridor. The TX was moved from the RX1 to the RX2 around the corner, and went from LOS to NLOS of RX1 and vice versa for RX2 link. In the corner the TX is being in LOS for both RX1 and RX2. A common reference was not feasible, hence the local rubidium clocks of the sounders were synchronized [2]. The height of the antennas was 160 cm for the TX and 190 cm for the RXs.

Fig. 4. The transmitter in the entrance hall.

The MIMO channel transfer function was sampled each 39.3216 ms, resulting in a number of transfer matrices $\mathbf{H} \in \mathbb{C}^{[r \times t \times f]}$. The movement of the TX was approximately

0.5 m/s, hence 30 snapshots represents approximately 10 wavelength. The total number of MIMO snapshots for the two links are > 7000 and covers a distance of about 38 m.
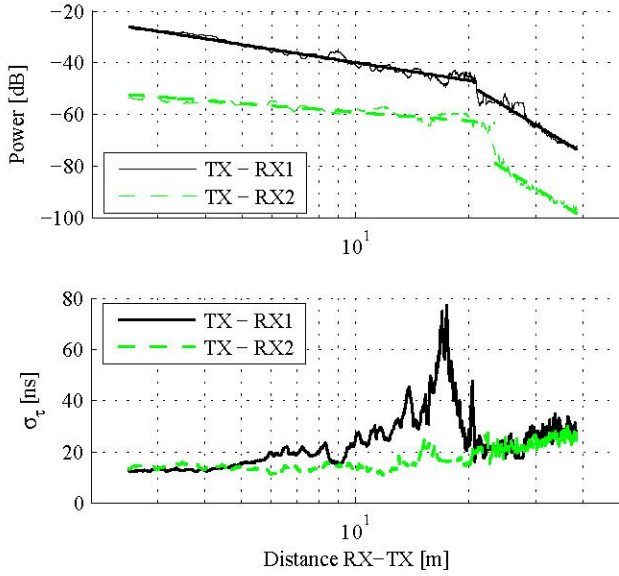

Fig. 5. Map of the measurement routes.

4 Measurement Results

In this section we present results based on the measurement campaign.

4.1 Delay Spread and Power Decay

In Fig. 6 the pathloss is plotted together with a least square line fit (the powers are not absolute, but biased for visibility reasons).[1] The pathloss exponents are for the $TX - RX1$: 2.2 and 8.2, and for $TX - RX2$: 1.5 and 9.7. In the figure we also present the delay spread as a function of distance estimated as [8]

$$\hat{\sigma}_\tau = \sqrt{\frac{\sum_{n=0}^{N-1} \hat{P}_h[n] \left(\frac{n}{BW}\right)^2}{\hat{P}_{\mathrm{mean}}} - \hat{\tau}_{\mathrm{mean}}^2}, \qquad (1)$$

where N is the number of MIMO snapshots and

$$\hat{P}_h[n] = \sum_{r=1}^{N_R} \sum_{t=1}^{N_T} |\mathbf{H}[r,t,n]|^2, \qquad (2)$$

where N_T and N_R are the number of transmitter and receiver elements, respectively, and where

$$\hat{\tau}_{\mathrm{mean}} = \frac{\sum_{n=0}^{N-1} \hat{P}_h[n] \frac{n}{BW}}{\hat{P}_{\mathrm{mean}}}, \qquad (3)$$

$$\hat{P}_{\mathrm{mean}} = \sum_{n=0}^{N-1} \hat{P}_h[n]. \qquad (4)$$

---

[1]Note that the distance is the moving distance and not the shortest distance between the TX and the RXs.

Fig. 6. Pathloss and delay spread as functions of moving distance for the two links.
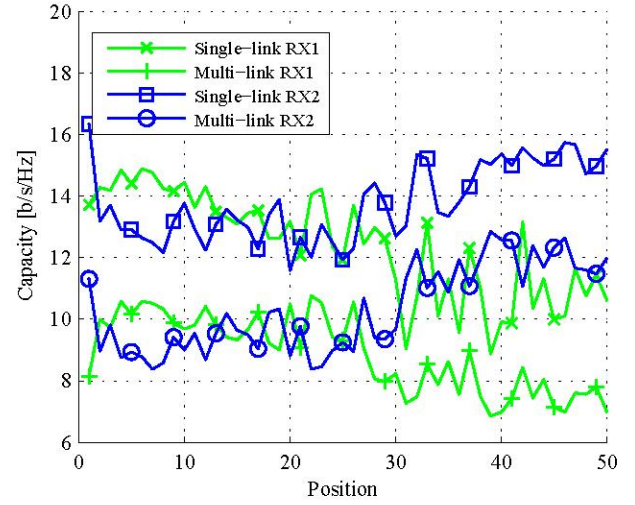

Fig. 7. Capacity with and without interference for the link of interest TX - RX1 (RX1) and TX - RX2 (RX2) with perfect power control, taken at 50 equidistant positions when TX is moved from RX2 to RX1 (see Fig. 5).

4.2 MIMO Capacity with Interference

In [3], MIMO capacity with interference is computed under the assumption that each user chooses his signaling without knowing the exact interference environment. With the focus on the user of interest the signal model for the narrow-band frequency sub-channel, k, for our setup becomes

$$\mathbf{y}_k = \sqrt{\rho}\mathbf{H}_{0,k}\mathbf{x}_k + \sum_{j=1}^{L}\sqrt{\eta_j}\mathbf{H}_{j,k}\mathbf{x}_{j,k} + \mathbf{n}_k, \qquad (5)$$

where $\mathbf{H}_{0,k}$ and $\mathbf{x}_{0,k}$ represent the channel matrix and the transmitted signal of the user of interest, respectively. It is assumed that the entries of the interfering channel transfer matrix $\mathbf{H}_{j,k}$ is independent from those of $\mathbf{H}_{j',k}$ if $j \neq j'$. The noise vector is assumed to have independent and identical distributed complex Gaussian entries. Then, for the L interferers, the interference plus noise is Gaussian distributed with an instantaneous covariance matrix

$$\mathbf{R}_{\mathrm{I},k} = \sum_{j=1}^{L}\eta_j\mathbf{H}_{j,k}\mathbf{H}_{j,k}^{H} + \mathbf{I}_{N_{\mathrm{R}}}. \qquad (6)$$

After pre-whitening the interference plus noise by multiplying $\mathbf{y}$ with $\mathbf{R}_{\mathrm{I},k}^{-1/2}$, the known results from [13, 9, 5] could be used to express the channel capacity between the input and output for the user of interest as [3]

$$C_k = \log_2\left[\det\left(\mathbf{I}_{N_{\mathrm{R}}} + \frac{\rho}{N_{\mathrm{T}}}\mathbf{H}_k\mathbf{H}_k^{H}\mathbf{R}_{\mathrm{I},k}^{-1}\right)\right]. \qquad (7)$$

First we assume perfect power control (normalized transfer matrices) for one link of interest $\mathrm{TX} - \mathrm{RX1}$ ($\mathrm{TX} - \mathrm{RX2}$) with one interfering link $\mathrm{TX} - \mathrm{RX2}$ ($\mathrm{TX} - \mathrm{RX1}$). In Fig. 7, we present the capacity for a 4×4 system for (i) a single-link

scenario where $\rho = 15$ dB and $\eta_1 = -\infty$ dB and (ii) for a multi-link scenario where $\rho = 15$ dB and $\eta_1 = 3$ dB.

In order to get an additional MIMO link, two TX positions were used, taken with a separation of 530 snapshots (approximately 10 m). TX2 is therefore about 10 m ahead of TX1. In Fig. 8, we plot the capacity of the channels with interference relative to the channels without interference. Both transmitters used the same transmit-power, and TX1 as well as TX2 was moving on the route from RX2 to RX1 (see Fig. 5). We assume perfect channel knowledge at the receivers and no channel knowledge at the transmitters. Each transmitter and each receiver used 4 antennas. I.e., there are four 4×4 MIMO channels in the evaluated multi-link MIMO-channel. In the investigated measurement, the link $\mathrm{TX1}-\mathrm{RX1}$ communicate "over" TX2 and therefore has larger interference than the link $\mathrm{TX1} - \mathrm{RX2}$ as seen in the figure. The average evaluation SIR varies between $-1\mathrm{dB}\cdots + 27\mathrm{dB}$ and $0\cdots + 21\mathrm{dB}$ for the MIMO channels $\mathrm{TX1} - \mathrm{RX2}$ and $\mathrm{TX2} - \mathrm{RX1}$, respectively. Consequently, the other two links ($\mathrm{TX1} - \mathrm{RX1}$ and $\mathrm{TX2} - \mathrm{RX2}$) had a SIR of $-21\mathrm{dB}\cdots 0\mathrm{dB}$ and $-27\mathrm{dB}\cdots + 1\mathrm{dB}$.

For the same scenario as in Fig. 8, the relative capacities as a function of the signal-to-interference ratio (SIR) are plotted in Fig. 9. A clear correlation between the SIR and the relative capacity is seen.

4.3 Interference Suppression

Here, we propose a simple metric for the multi-link MIMO channel interference robustness. We use the SIR after spatial filtering the interference transfer matrix with the singular vector associated with the largest singular value; the mode associated with the largest singular value contributes most to the capacity and is the one also used in MRC/MRT schemes.
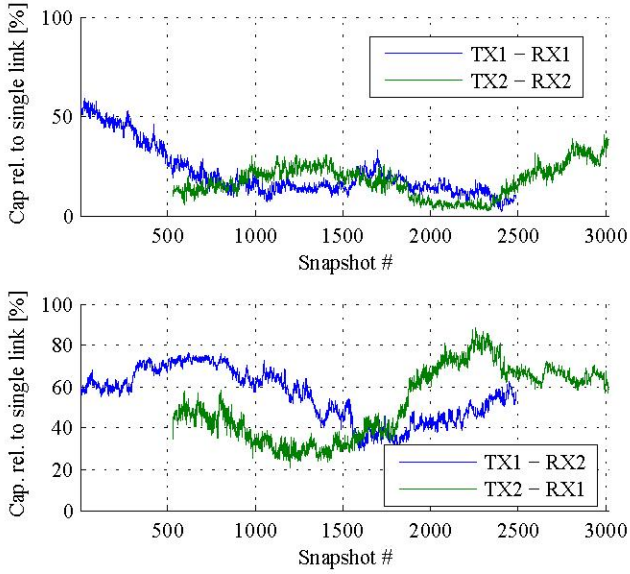
Fig. 8. Capacity with interference relative to single-link system without interference, as a function of snapshots. No power control is used and TX is moved from RX2 to RX1 (see Fig. 5).
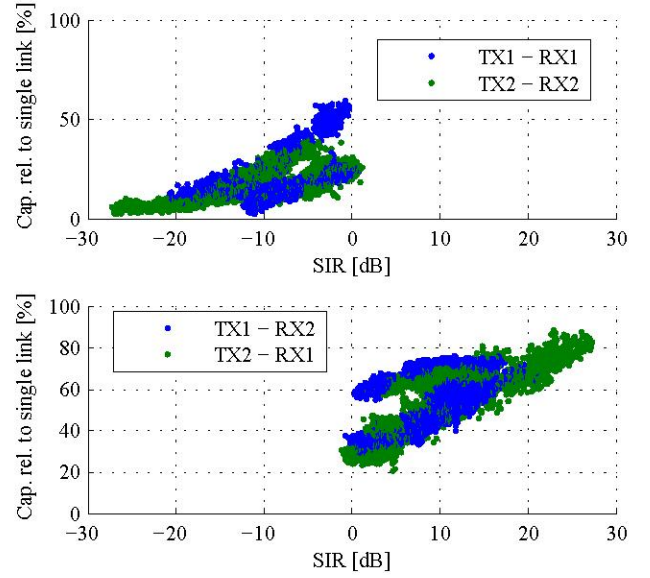
Fig. 9. Capacity with interference relative to single-link system without interference, as a function of SIR. No power control is used and TX is moved from RX2 to RX1 (see Fig. 5).

The power of the channel mode of interest is for the normalized transmfer matrix

$$P_0 = \mathbf{u}_{0,1}^H \mathbf{H}_0 \mathbf{v}_{0,1} = s_{0,1}^2, \qquad (8)$$

where $\mathbf{u}_{0,1}$ corresponds to the singular vector of the largest singular value. The power of the interference after spatial filtering is then for the L normalized transfer matrices

$$P_{\mathrm{I}} = \left\| \mathbf{u}_{0,1}^H \sum_{j=1}^{L} \mathbf{H}_j \right\|_{\mathrm{F}}^2, \qquad (9)$$

where $\| \bullet \|_{\mathrm{F}}$ is the Frobenius norm. The channel SIR for the normalized transfer matrices is then

$$\gamma_{\mathrm{I}} = \frac{P_0}{P_{\mathrm{I}}}. \qquad (10)$$

In Fig. 10, we plot the P_0 and P_I and γ_I for 50 positions when the TX is moved from RX1 to RX2 (see Fig. 5).
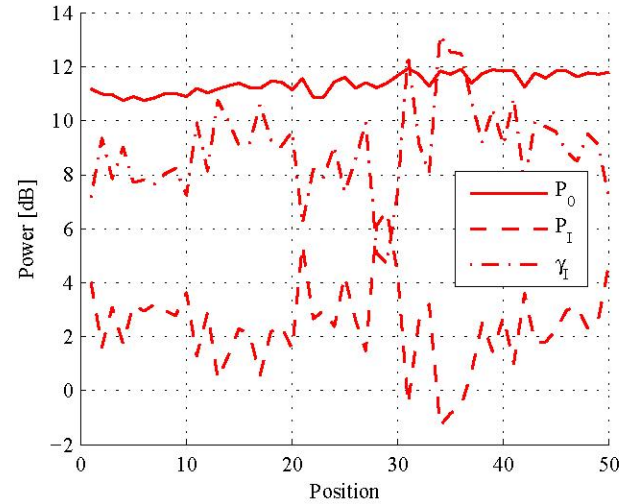

Fig. 10. Interference suppression for the 4×4 TX − RX1 link, taken at 50 equidistant positions when TX is moved from RX2 to RX1 (see Fig. 5).

5 Conclusions

In this paper we presented a dynamic multi-link wideband MIMO channel indoor measurement campaign at 5.3 GHz. The system setup was described and basic measures as path-loss and delay spreads were given as functions of the distance for a scenario where transmitter was moving from a large entrance hall to a typical office corridor at the premises of Lund University.

Further, capacity with interference (with and without power control) results based on the dynamic multi-link MIMO measurements were shown and also the capacity with interference relative to the non-interference capacity as a function of SIR. Here we experienced a strong correlation between the relative

capacity and SIR. Finally, an interference suppression metric is introduced and evaluated on the measured data.

References

[1] http://www.channelsounder.de/ruskchannelsounder.html.

[2] P. Almers, S. Wyne, F. Tufvesson, and A. F. Molisch, "Effect of Random Walk Phase Noise on MIMO Measurements," in *Proceedings IEEE VTC-Spring*, vol. 1, Stockholm, Sweden, 2005, pp. 141–145.

[3] R. S. Blum, "MIMO capacity with interference," *IEEE Journal on Selected Areas in Communications*, vol. 21, no. 5, pp. 793–801, June 2003.

[4] G. Caire and S. Shamai, "On the achievable throughput of a multiantenna gaussian broadcast channel," *IEEE Transactions on Information Theory*, vol. 49, no. 7, pp. 1691–1706, July 2003.

[5] G. J. Foschini and M. J. Gans, "On limits of wireless communications in fading environments when using multiple antennas," *Wireless Personal Communications*, vol. 6, no. 3, pp. 311–335, March 1998.

[6] M. Jeng-Shiann Jiang; Demirkol, M.F.; Ingram, "Measured capacities at 5.8 GHz of indoor MIMO systems with MIMO interference," in *Proceedings IEEE VTC-Fall*, vol. 1, October 2003, pp. 388–393.

[7] V.-M. Kolmonen, J. Kivinen, L. Vuokko, and P. Vainikainen, "5.3-GHz MIMO radio channel sounder," *IEEE Transactions on Instrumentation and Measurement*, vol. 55, no. 4, pp. 1263–1269, Aug. 2006.

[8] A. F. Molisch, *Wireless communications*, 1st ed. IEEE Press – Wiley, 2005.

[9] I. E. Telatar, "Capacity of Multi-Antenna Gaussian Channels," *Technical Memorandum, Bell Laboratories, Lucent Technologies*, October 1998, published in *European Transactions on Telecommunications*, vol. 10, no. 6, pp. 585–595, November/December 1999.

[10] R. Thoma, D. Hampicke, A. Richter, G. Sommerkorn, A. Schneider, U. Trautwein, and W. Wirnitzer, "Identification of time-variant directional mobile radio channels," *IEEE Transactions on Instrumentation and Measurement*, vol. 49, no. 2, pp. 357–364, April 2000.

[11] S. Verdu, "Multiple-access channel with memory with and without frame synchronism," *IEEE Transactions on Information Theory*, pp. 605–619, May 1989.

[12] H. Weingarten, Y. Steinberg, and S. Shamai, "The capacity region of the gaussian multiple-input multiple-output broadcast channel," *IEEE Transactions on Information Theory*, vol. 52, no. 9, pp. 3936–3964, September 2006.

[13] J. H. Winters, "On the capacity of radio communications systems with diversity in Rayleigh fading environments," *IEEE Journal on Selected Areas in Communications*, vol. 5, pp. 871–878, June 1987.

[14] W. Yu and J. Cioffi, "Trellis precoding for the broadcast channel," in *Proceedings IEEE GLOBECOM*, vol. 2, November 2001, pp. 1344–1348.

[15] W. Yu, W. Rhee, S. Boyd, and J. Cioffi, "Iterative water-filling for Gaussian vector multiple-access channels," *IEEE Transactions on Information Theory*, vol. 50, no. 1, pp. 145–152, January 2004.